High-Impedance Surfaces With Periodically Perforated Ground Planes

Ahmet Cemal Durgun, *Member, IEEE*, Constantine A. Balanis, *Life Fellow, IEEE*, Craig R. Birtcher, Hai Huang, and Hongyu Yu, *Member, IEEE*

***Abstract*—Because of the design limitations of conventional high-impedance surfaces (HIS), it is not possible to miniaturize the HIS and increase the bandwidth, simultaneously. To overcome this, a novel HIS is proposed with a periodically perforated ground plane. The magnetic flux flowing through the perforations results in an extra inductance which increases the fractional bandwidth and decreases the center frequency. Since the perforated HIS can also be considered as a defected ground structure (DGS), surface wave suppression can also be achieved by properly determining the geometry of the perforations. Therefore, a bandgap can be obtained without the need of vias, which considerably increase fabrication costs. It is also possible to tune and overlap the reflection phase and surface wave suppression bands. However, due to the rotational asymmetry of the structure, surface wave suppression is achieved in only one direction.**

***Index Terms*—Bandwidth enhancement, electromagnetic bandgap (EBG), high-impedance surface (HIS), miniaturization, surface wave suppression.**

I. Introduction

THE last years of the twentieth century has witnessed the birth of a novel and extremely useful electromagnetic device, referred to as high-impedance surface (HIS) or electromagnetic band gap (EBG) structure [1], [2], which are utilized for low-profile antenna applications and surface wave suppression [1]–[15].

For low-profile antenna applications, the thickness of the substrate is usually chosen to be much smaller than the operating wavelength. In addition, in most cases, the size of the ground plane is finite and limited to the available space, which affects the performance of an antenna mounted on it. The size of the unit cell is also important in terms of the dependency of the reflection characteristics to the angle of incidence. It is already known that the sensitivity of an HIS to the angle of incidence decreases with the unit cell size [16]. That is, compactness of an HIS can be extremely significant for some cases. On the other hand, a large bandwidth has always been a preferred property for most of the RF systems. Therefore, it is always desirable to design an HIS with large bandwidth, thin substrate and small unit cell size.

HIS unit cell miniaturization can be accomplished by utilizing different types of patches, including spiral [17], slotted [3] and space filling curve [18] type patches, instead of square ones. Nevertheless, the immediate shortcoming of these HISs is the bandwidth reduction. In fact, for a given substrate thickness and patch width, the maximum bandwidth can be achieved by square patches [15]. Thus, because of the design limitations of a conventional HIS, it is not possible to miniaturize the surface and enhance its bandwidth, simultaneously.

Another advantage of EBG structures is their surface wave (SW) suppression capabilities. Wave propagation, within the substrate, can be prevented in several ways. One of them is perforating the dielectric by periodic dielectric inclusions or metallic posts referred to as *vias* [1], as in the case of a mushroom surface. In the literature, there are various successful applications of mushroom surfaces [1]–[9]. However, there are basically two drawbacks of these structures. First, since the copper plated through holes are very vulnerable to bending, vias should be avoided in flexible or conformal applications. Second, the maximum SW suppression and AMC bands of these surfaces do not overlap all the time, and trying to overlap those bands may be highly troublesome for certain designs, especially with thin substrates. Finally, inclusion of vias increases the cost of fabrication.

There are other types of EBG structures in which the vias are eliminated but surface wave suppression is still possible. A very common example of such a structure is uniplanar compact photonic band gap (UCPBG) structure [19], [20]. In these surfaces, the patches are notched in a rectangular form and are electrically connected by very thin lines which pass through their centers. This results in an equivalent inductance, and the vias can be eliminated. Therefore, it is much easier and cheaper to fabricate these structures. Yet, they have narrower reflection phase bandwidth compared to HISs with square patches [15]. Besides, the overlapping problem of SW suppression and AMC bands is still unresolved.

Another physical realization of an EBG structure, without vias, is defected ground structures (DGS). In DGSs, some part of the ground plane is etched away to obtain the band gap. DGSs are generally used for microstrip filter design [21]–[24]. They are also used to decrease the coupling between microstrip antennas [25] and lines [26], to eliminate scan blindness [27], to control harmonic radiation of microstrip antennas [28], [29], etc.

Manuscript received July 22, 2013; revised March 24, 2014; accepted May 22, 2014. Date of publication June 18, 2014; date of current version September 01, 2014. This work was supported by the ASU Advanced Helicopter Electromagnetics (AHE) Program.

A. C. Durgun is with the School of Electrical, Computer, and Energy Engineering, Arizona State University, Tempe, AZ 85287 USA, and also with Intel Corporation, Chandler, AZ 85226 USA (e-mail: adurgun@asu.edu).

C. A. Balanis, C. R. Birtcher, and H. Yu are with the School of Electrical, Computer, and Energy Engineering, Arizona State University, Tempe, AZ 85287 USA (e-mail: balanis@asu.edu; craig.birtcher@asu.edu; hongyuyu@asu.edu).

H. Huang is with the School of Electrical, Computer and Energy Engineering, Arizona State University, Tempe, AZ 85287 USA, and also with Lorentz Solution Inc., Santa Clara, CA 95054 USA (e-mail: hhuang60@asu.edu).

Color versions of one or more of the figures in this paper are available online at http://ieeexplore.ieee.org.

Digital Object Identifier 10.1109/TAP.2014.2331703

However, one drawback of DGSs is that they do not have artificial magnetic conductor (AMC) properties.

The limitations on the bandwidth of the conventional HISs led the authors to the quest of a novel geometry which solves the miniaturization and bandwidth enhancement problems, simultaneously. Indeed, this can be accomplished by perforating the ground plane periodically, as shown in Fig. 1. This type of a structure was previously considered in [16] to miniaturize single layer frequency-selective surfaces (FSS) and its transmission properties were discussed. However, in this paper, the structure is considered as an AMC ground plane, which is proposed to decrease the operating frequency and increase the bandwidth of two-layer HISs. Its reflection properties are investigated and compared with those of the conventional HISs. Furthermore, similar to the UCPBG and DGS structures, the HIS with a periodically perforated ground plane is verified to be capable of suppressing SWs. This can be accomplished by designing the geometry of the perforations properly. Hence, vias can be eliminated without hindering the EBG or AMC properties and the structure can be designed such that both SW suppression and AMC bands do overlap.

The organization of the paper is as follows. In the second part, basic design limitations of conventional HISs are reviewed. In the third part, the geometry of the new HIS is given and an analytical transmission line model is explained. The fourth part is dedicated to the reflection properties of the surfaces, which is followed by a discussion on the SW propagation within the substrate and experimental verification. Finally, the work is summarized together with concluding remarks.

II. Design Limitations of HIS

Design limitations of HISs can be understood by examining their physical geometry and analytical model. Although there are several quantitative methods that are already reported in the literature [30]–[32], a qualitative approach will be followed here to summarize those results.

A conventional HIS is composed of a periodically arranged array of metallic patches mounted on a grounded dielectric substrate, and it can be modeled by a parallel LC circuit provided that the periodicity of the surface is much smaller than the wavelength at the operating frequency [1]. Hence, the center frequency and the bandwidth are proportional to $1\sqrt{(LC)}$ and $\sqrt{L/C}$, respectively. The capacitance of the surface is due to the gap between the conducting plates on the top of the dielectric substrate and the inductance is due to the ground plane in close proximity to the array of patches. In the literature, there are several analytical models and expressions for the equivalent inductance and capacitance of an HIS [1], [33], [34]. All of those models approach the problem from a different direction and end up with different expressions. However, it is common in all of them that the capacitance depends on the patch size and proximity. On the other hand, the inductance and fractional bandwidth depend only on the thickness of the substrate [1]. Because of this reason, the basic limitation in the design procedure is on the bandwidth.

For a fixed substrate thickness, we do not have control of center frequency and bandwidth at the same time. Once either the center frequency or the bandwidth is specified, the other

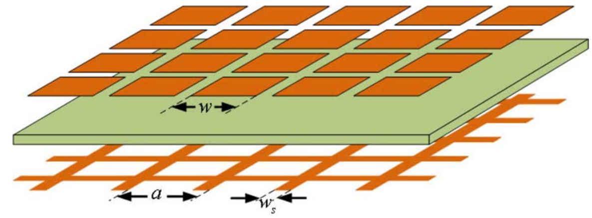

Fig. 1. Physical geometry of an HIS with periodically perforated ground plane. On top, there is the capacitive array of metallic patches. The second layer is the dielectric substrate. The bottom layer is the inductive grid.

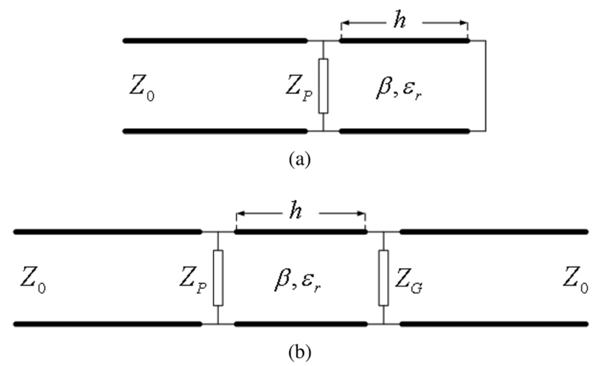

Fig. 2. Transmission line model of the HIS. (a) Conventional HIS (b) New HIS with the perforated ground plane.

depends upon it. Furthermore, the entire frequency range cannot be covered by using reasonable patch dimensions.

Low-profile applications usually exhibit small bandwidths because of thin substrates. Moreover, since the inductance of a conventional HIS depends only on the thickness, the frequency of operation can be tuned by varying the capacitance of the surface. Expectedly, relatively lower operating frequencies can be achieved only by increasing the capacitance of the surface. This can be realized by decreasing the gap between the patches, increasing the patch size and/or using the aforementioned patch geometries. However, this either contradicts with the compactness or large bandwidth requirements. Consequently, it is not possible to miniaturize unit cell and enhance the bandwidth at the same time.

III. Design Geometry and Analytical Model

The square root of surface inductance is directly proportional to the bandwidth and inversely proportional to the center frequency of an HIS. Hence, if the inductance of an HIS can be increased without changing its unit cell dimensions and thickness, a lower resonant frequency and a wider bandwidth can be achieved. This can be implemented by perforating the ground plane periodically, as illustrated in Fig. 1. The ground plane can also be considered as a metallic grid composed of strips of width w_s. In this structure, the perforations allow the magnetic flux, generated by the currents circulating around the grid, to flow through the holes and this results in an extra inductance. This additional inductance increases the equivalent inductance of the overall structure, resulting in a lower resonant frequency and larger bandwidth.

A transmission line model can be developed for the new HIS as shown in Fig. 2 where Z_P and Z_G denote the impedances of the array of patches and the perforated ground plane, respectively. The dielectric layer behaves as an impedance transformer

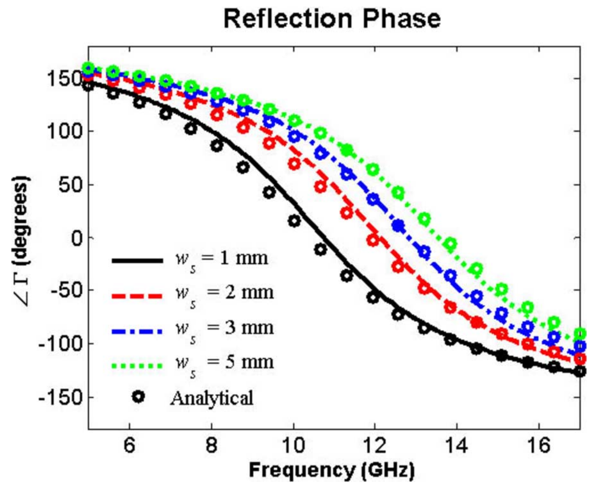

Fig. 3. Comparison of the simulated and analytical reflection phase for different strip widths.

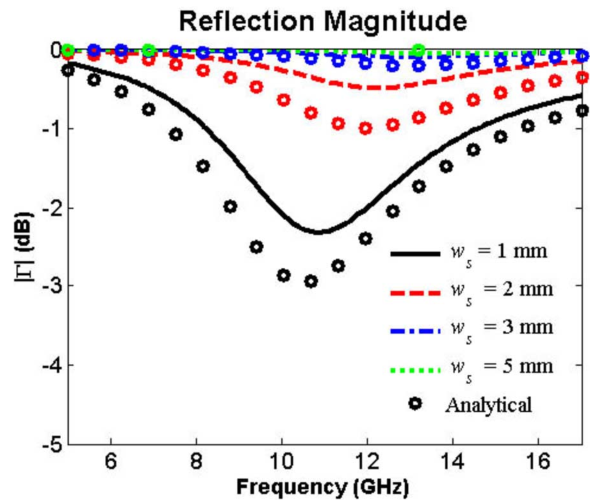

Fig. 4. Magnitude of the reflection coefficient for different strip widths.

of length h, which is the thickness of the substrate. Z_0 is the wave impedance in the surrounding medium which is a function of the angle of incidence and the polarization of the incident field. Z_P and Z_G are given in [33], and they are going to be repeated here for the sake of completeness.

$$Z_P^{TM} = -j\frac{\eta_{eff}}{2\alpha_P} \tag{1}$$

$$Z_P^{TE} = -j\frac{\eta_{eff}}{2\alpha_P\left(1-\frac{k_0^2}{k_{eff}^2}\frac{\sin^2\theta}{2}\right)} \tag{2}$$

$$Z_G^{TM} = j\frac{\eta_{eff}}{2}\alpha_G\left(1-\frac{k_0^2}{k_{eff}^2}\frac{\sin^2\theta}{2}\right) \tag{3}$$

$$Z_G^{TE} = j\frac{\eta_{eff}}{2}\alpha_G. \tag{4}$$

The expressions for the grid parameters for the array of patches (α_P) and for the perforated ground plane (α_G) are as follows:

$$\alpha_P = \frac{k_{eff}a}{\pi}\ln\left(\frac{1}{\sin\frac{\pi(a-w)}{2a}}\right) \tag{5}$$

$$\alpha_G = \frac{k_{eff}a}{\pi}\ln\left(\frac{1}{\sin\frac{\pi w_s}{2a}}\right). \tag{6}$$

When the surrounding medium is air, the effective permittivity is approximated by (7), where ϵ_r is the relative permittivity of the dielectric layer:

$$\varepsilon_{eff} = \frac{\varepsilon_r+1}{2}. \tag{7}$$

It is obvious that, while the array of patches has a capacitive impedance, the impedance of the perforated ground plane is inductive. The equivalent capacitance of the surfaces increases with the patch width (w). On the other hand, the inductance decreases as the strip width (w) increases. In other words, larger surface inductances can be obtained by larger perforations. Because the magnitude of the magnetic flux flowing through the ground plane increases with the perforation size, it results in a larger equivalent inductance.

IV. Reflection Phase

In order to observe the reflection properties of the proposed HIS, one sample is designed and simulated by HFSS[1]. The unit cell size (a) and the patch width (w) are selected to be 5 and 4.1 mm, respectively. The dielectric material is Rogers RT/duroid 5870[2] with a dielectric constant of 2.33 and thickness of 1.524 mm. The widths of the strips are varied from 1 to 3 mm and the effects of the strip width on the center frequency and bandwidth are investigated. The center frequency is assumed to be the point where the surface behaves as a perfect magnetic conductor (zero reflection phase). The bandwidth is considered as the frequency interval where the reflection phase takes values between $+90^\circ$ and -90°.

Fig. 3 shows the reflection phase of the new HIS for different strip widths and that of the conventional HIS with identical unit cell dimensions. Note that the case $w_s = 5$ mm corresponds to the conventional HIS. The numerical results are also compared with the analytical ones obtained by the transmission line model discussed in the pervious section. The numerical solutions are obtained by simulating a single unit cell of the HIS.

The agreement between the analytical and numerical models is excellent for this specific geometry. The agreement may not be very good for some other designs as the analytical formulation is not proved to be valid for any HIS. However, (1) through (7) can still be used to obtain an initial design. The designs can then be fine tuned by numerical simulations.

As expected, the width of the strips, or the perforation size, has a very significant effect on the reflection characteristics of the surface. Clearly, the center frequency of the surface decreases with the strip width. On the other hand, the fractional bandwidth increases as strip width decreases. Hence, without changing the physical dimensions of a unit cell, we can achieve lower frequencies of operation and larger bandwidths, simultaneously, by decreasing the strip width. However, as the size of the holes within the ground plane is increased, more energy is allowed to leak to the other side of the HIS. Therefore, the magnitude of the reflection coefficient, within the operational bandwidth, decreases with the strip width. Fig. 4 exhibits a compar-

[1][Online]. Available: http://ansoft.com/Products/

[2][Online]. Available: http://www.rogerscorp.com/products/index.aspx

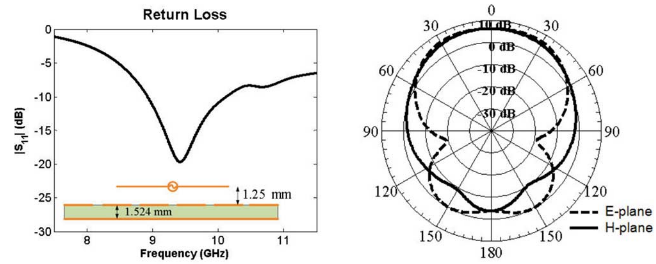

(a) (b)

Fig. 5. Return loss and radiation pattern of a dipole located on top of a PHIS. One side of the PHIS is $1.8\ \lambda$ in length. (a) Return loss. (b) Radiation pattern.

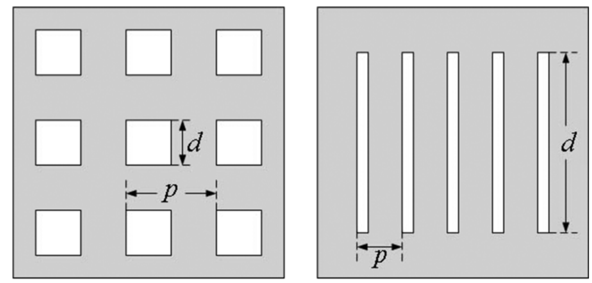

(a) (b)

Fig. 6. Schematic drawing of the defected ground structures. (a) Type 1 ($p > d$). (b) Type 2 ($d > p$).

TABLE I
REFLECTION CHARACTERISTICS OF THE PROPOSED HIS.

	f_0 (GHz)	a (λ_0)	BW (%)	$\|\Gamma\|$ (dB)
$w_s = 5.0$ mm	13.5	0.225	40.7	-0.06
$w_s = 3.0$ mm	13.0	0.217	41.5	-0.10
$w_s = 2.0$ mm	12.0	0.200	43.3	-0.50
$w_s = 1.0$ mm	10.7	0.178	48.6	-2.30

ison of the analytical and numerical models for different strip widths. Apparently, the analytical model overestimates the loss.

Table I summarizes the simulation results that verify the compromise between bandwidth improvement and reflected power. Hence, a designer should take into account the amount of leakage that can be tolerated to determine the size of the perforations and unit cell dimensions. For instance, for the given design, it is possible to obtain a 20.7% decrease in the center frequency and 7.9% bandwidth improvement at an expense of 2.3 dB reduction in the magnitude of the reflection coefficient. On the other hand, in low-profile antenna applications, HISs are generally operated in their inductive region [3], which also provides antenna miniaturization [12]. Therefore, for such an application, the amount of power loss should be smaller. For instance, if a $0.375\ \lambda$ dipole is located at a $0.04\ \lambda$ distance above the PHIS, with strip width (w_s) of 1 mm, the dipole resonates around 9.43 GHz, and the magnitude of the reflection coefficient of the PHIS, at this frequency, is -1.8 dB. Fig. 5 shows the simulated return loss and the E- and H-plane radiation patterns of the dipole. The PHIS is square in shape with a side length of 12 cells $(1.8\ \lambda)$. The gain of the structure is 5.5 dBi, which compares well with the other examples, reported in [4], that utilize conventional HISs. However, the reader should always keep in mind that, due to the perforations on the ground plane, the back lobe radiation is relatively high compared to a case where a conventional HIS used.

V. SURFACE WAVE SUPPRESSION

Since the PHIS can also be considered as a DGS loaded with a periodic array of patches, SW suppression can be achieved by judiciously determining the geometry of the defects. It is also important to overlap the AMC and SW suppression bands.

DGSs can be separated into two groups. The first one is a periodic structure which is based on *Bragg's Diffraction* phenomenon. The second group, not necessarily a periodic structure, is composed of defects which form an equivalent LC filter. The inductance is due to the extra magnetic flux flowing through the holes and the capacitance is due to the charges accumulating around the gaps.

Fig. 6 displays two different types of DGSs. In the first one, the periodicity of the defects is larger than the width of the defects $(p > d)$. For this type, the rejection of waves is due to the Bragg's diffraction and the stop band occurs when $p \approx \lambda/2$[21]. When the distance between the defects is around a half wavelength, the fields reflected from each defect interacts constructively resulting in a strong reflection. Thus, to achieve a SW suppression, the distance between the perforations should be approximately half wavelength at the operating frequency.

In the second type, the width of the defects is larger than the periodicity $(d > p)$. For this case, the slots (defects) reach resonance (infinite impedance) before the Bragg's diffraction takes place and the propagating fields are reflected back because of the high impedance per unit length [24]. This type of DGSs are also referred to as *High Impedance Wires* [24], when they are utilized in microstrip line applications. The stop band occurs when $d \approx \lambda$[24]. The defects behave like short-circuited stubs, and when the length from the center of the slot to the shorted end is approximately half wavelength, the impedance gets very high and the power is reflected back. The basic advantage of such a structure is its compactness [23].

In this paper, the authors opted to utilize the defects of Type 2 because of their compactness. A slot defect, which is folded in the form of a split ring, for this type of an application, has already been reported in the literature [35]. Although promising results were obtained in terms of SW suppression, power loss was a serious issue for that design. Hence, in this work, a dumbbell type defect, which allows further miniaturization and compactness, is used. The structure was designed to operate at its second band to get rid of the excess power loss. To overlap the SW suppression and AMC bands, the size of the perforations were designed to be larger than the periodicity of the patches. The patches and perforations, together, form a larger super-cell, as illustrated in Fig. 7.

Fig. 8 displays the dispersion diagram of the PHIS along the direction perpendicular to the narrow slots. According to the dispersion diagram, the PHIS exhibits a stop band between 12.4 and 13.0 GHz. As explained before, this is the second stop band of the PHIS, which is between 2^{nd} and 3^{rd} modes. The first band gap occurs before the 2^{nd} mode crosses the light line.

SW suppression properties of the PHIS were verified by several simulations. In the first one, the coupling between two parallel microstrip lines was simulated when there is the PHIS be-

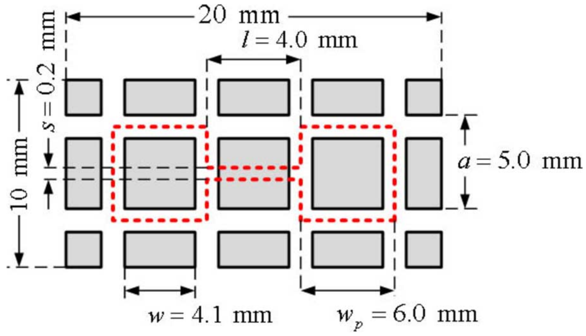

Fig. 7. Schematic drawing of a single super-cell of the PHIS. The dashed lines show the boundary of the perforation which is on the bottom of the substrate.

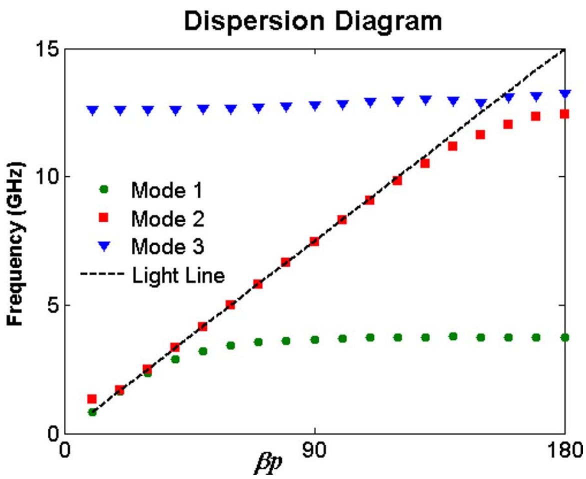

Fig. 8. Dispersion diagram of the PHIS obtained by a full-wave simulation.

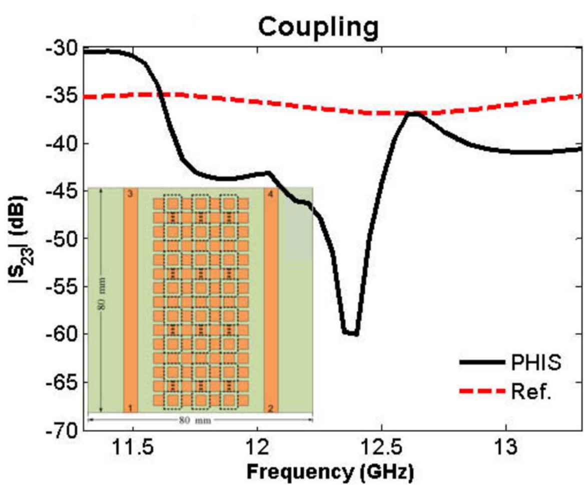

Fig. 9. Coupling reduction between two microstrip lines.

tween them, and compared with the reference case, where there is nothing between the two lines. The 50 Ω transmission lines were designed on a Rogers RT/duroid 5870 substrate. The distance between the edges of the transmission lines was recorded as 45.5 mm. Fig. 9 shows the coupling reduction between ports 2 and 3, which are enumerated on the schematic drawing of the simulation geometry. Apparently, there exists a bandgap between 11.7 and 12.5 GHz

The next example is the demonstration of coupling reduction between two probe fed microstrip patch antennas. The antennas were designed to operate around 12.3 GHz. The geometry of the

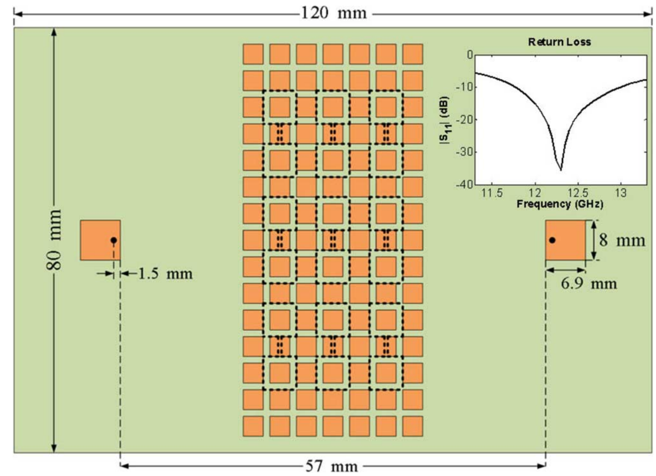

Fig. 10. Schematic drawing of the simulation geometry to demonstrate the coupling reduction between the microstrip patch antennas. The antennas operate around 12.3 GHz.

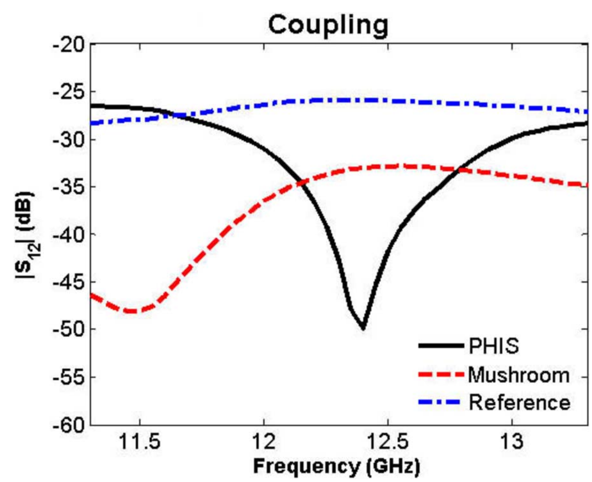

Fig. 11. Comparison of the mutual coupling between the antennas for three different cases. Reference: There is no structure between the antennas. Mushroom: A conventional mushroom surface between the antennas. PHIS: Perforated HIS between the antennas.

simulation and the simulated return loss of the antennas are illustrated in Fig. 10. The mutual coupling between the microstrip antennas was simulated for three different cases, as shown in Fig. 11. In the figure, *PHIS* and *Mushroom* , respectively, denote the cases where there is the proposed PHIS and the conventional mushroom surface, with exactly identical patch width and periodicity, between the antennas. Similarly, for the reference case, there is not any structure between the antennas. The radius of the vias of the mushroom surface is 0.25 mm. Clearly, the PHIS exhibits a very nice bandgap around the center frequency of the antennas. On the other hand, the bandgap of the mushroom surface occurs around 11.5 GHz.

The phase and the magnitude of the reflection coefficient of the PHIS can be seen in Fig. 12. The electric field is polarized in the direction perpendicular to the narrow slots on the ground plane. Apparently, the magnitude of the reflection coefficient is around -0.7 dB near the center frequency, and it is below -1 dB within the entire band. Also, the AMC and SW suppression bands of the PHIS do overlap. Nonetheless, this is not true for the mushroom surface. Although the reflection phase center

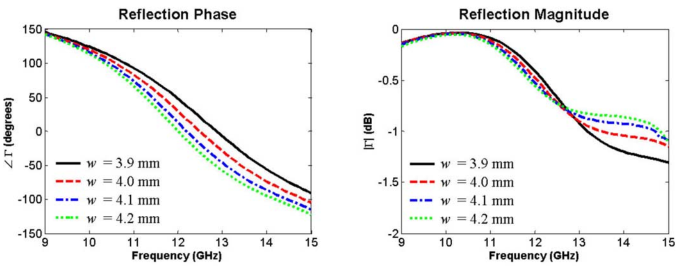

(a) (b)

Fig. 12. Phase and magnitude of the reflection coefficient of the PHIS for different patch widths. The electric field is polarized in the direction perpendicular to the narrow slots. (a) Phase. (b) Magnitude.

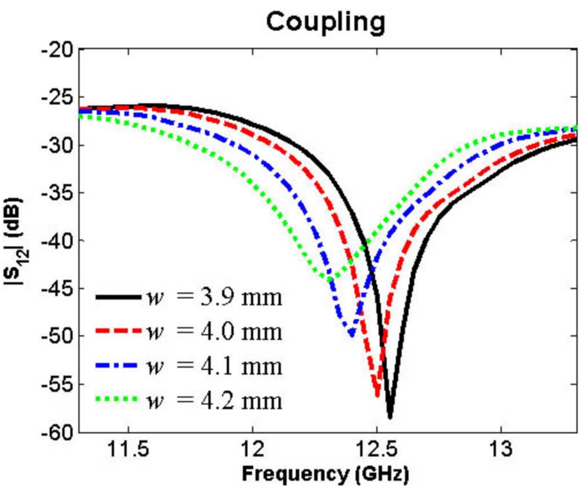

Fig. 13. Variation of the EBG band as a function of patch width.

frequency of the mushroom surface is 13.5 GHz, as stated in Table I, the bandgap is around 11.5 GHz.

EBG band of the PHIS definitely depends on the size and geometry of the perforations. In addition, position of the bandgap is also a function of the size of the patches on the top surface of the PHIS. This is attributed to the slow wave effect of the patch loading. Fig. 13 displays the variation of the bandgap of the PHIS with respect to the patch width. As expected, the bandgap moves to lower frequencies as the patch width increases. Obviously, this results in a miniaturization of the surface, i.e., the EBG band of a PHIS occurs at a lower frequency compared to a conventional DGS.

If we compare the variation of the AMC and SW suppression bands with respect to the patch width, we can see that the variation in the reflection phase is larger. For this particular example, as the patch width changes between 3.9 mm and 4.2 mm, the reflection phase shifts from 12.9 GHz to 12 GHz, while the bandgap shifts from 12.55 GHz to 12.3 GHz. The difference in the amount of variation of the two bands makes it possible to tune and overlap them.

The reflection and SW suppression properties of perforated structures are subject to change when other objects are placed in close proximity. However, since the PHIS is designed to minimize the power transmitted through the perforations, the impact of the presence of the other objects are also minimized. For example, placing a metallic layer of copper shifts the EBG resonance at most 150 MHz when the distance between the PHIS and the metallic layer is 0.1λ or greater. On the other hand, when the distance is 0.08λ, the resonance shifts approximately 300 MHz and there is 15 dB reduction in the coupling. Clearly, the PHIS can be designed by taking into consideration these resonance shifts due to the presence of the metallic layer.

At this point, it is worth mentioning one drawback of the PHIS with dumbbell shaped perforations. Due to the charges accumulated around the narrow slot, the capacitance of the PHIS is increased compared to the conventional HIS. Consequently, the reflection phase bandwidth has been reduced from 40.7% to 27.9%. Thus, we can conclude that there is compromise between SW suppression and bandwidth.

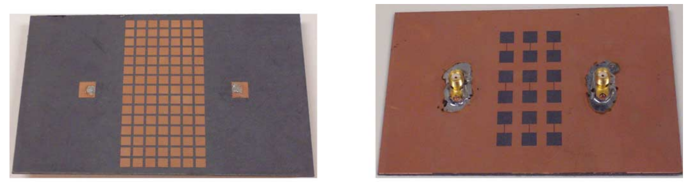

(a) (b)

Fig. 14. Photographs of the fabricated PHIS and microstrip patch antennas. (a) Top view. (b) Bottom view.

VI. Experimental Verification

For the experimental verification of the claimed properties, the setup shown in Fig. 10 was fabricated by using Rogers RT/duroid 5870 high frequency laminate cladded with 0.5 oz. (17 μm) copper layer on both sides, as the substrate. The top and bottom layers of the setup was patterned by standard photolithography process followed by wet etching of copper. The photoresist and the copper etchant were AZ4620 and Transene CE-100, respectively. EVG620 mask aligner was used for UV light exposure. Fig. 14 illustrates the top and bottom views of the fabricated structure.

After fabrication of the experiment setup, the mutual coupling between the antennas was measured for four different cases and the results were compared with simulations. An HP8510C Vector Network Analyzer was used as the instrumentation at the Arizona State University ElectroMagnetic Anechoic Chamber facility. The measured data was acquired at 801 frequency points between 11.3 and 13.3 GHz. A synthesized source was operated in step frequency mode, and an IF averaging factor of 2048 was used. The comparisons of the measurements and simulations are illustrated in Fig. 15. It can be observed that maximum SW suppression occurs at 12.55 GHz, instead of the design frequency (12.30 GHz). This frequency shift is basically because of the accuracy of the fabrication process, particularly the undercut and nonuniformity of the etching. When the patch width and the perforation sizes are adjusted to 4.05 mm and 5.9 mm, respectively, a good agreement between simulations and measurements can be obtained. Indeed, those values are well within the reasonable range, as far as the accuracy of the fabrication is considered.

Another interesting point that is worth mentioning is that SWs are not suppressed when there is only perforations between the antennas. Indeed, the stopband of the DGS occurs at a higher frequency. However, for the PHIS case, due to the slow wave effect of the patch array, the stopband is shifted to 12.55 GHz.

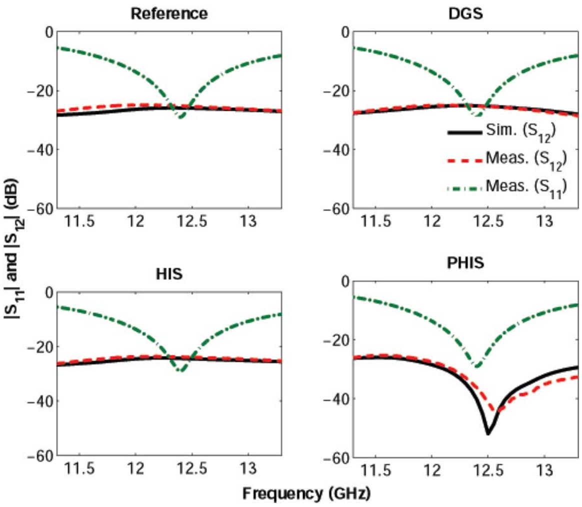

Fig. 15. Comparison of the simulations and measurements for four different cases. Reference: Nothing between the antennas. DGS: Only perforated ground plane between the antennas. HIS: Only conventional HIS (no vias) between the antennas. PHIS: Perforated HIS between the antennas.

VII. Conclusions

A new type of HIS is proposed with a perforated ground plane. It has been verified that the extra magnetic field flux flowing through those perforations increases the equivalent inductance of the surface which increases the bandwidth. Therefore, it is possible to miniaturize the unit cell and enhance the bandwidth at the same time, the inability of which is the major limitation of conventional HISs. The bandwidth increases (the center frequency decreases) as the size of the perforations increases. However, there is a compromise between bandwidth improvement (compactness) and reflected power. It has been also demonstrated that a bandgap can be obtained by judiciously designing the geometry of the defects. Thus, it is possible to eliminate metallic posts, which increase the fabrication costs, without hindering SW suppression capabilities. However, the bandgap is not a complete one, due to the rotational asymmetry. In addition, the AMC and SW suppression bands can be tuned to overlap. It is also possible to decrease the amount of power loss, due to the perforations, by operating the PHIS in its second band. Besides, a performance reduction in terms of miniaturization and bandwidth enhancement is observed when the perforations are designed to suppress SWs.

References

[1] D. Sievenpiper, "High-impedance electromagnetic surfaces," Ph.D., Dept. of Elect. Eng., Univ. of California Los Angeles, Los Angeles, CA, USA, 1999.

[2] C. A. Balanis, *Advanced Engineering Electromagnetics*, 2nd ed. Hoboken, NJ, USA: Wiley, 2012.

[3] F. Yang and Y. Rahmat-Samii, "Reflection phase characterizations of the EBG ground plane for low profile wire antenna applications," *IEEE Trans. Antennas Propag.*, vol. 51, no. 10, pp. 2691–2703, Oct. 2003.

[4] F. Yang and Y. Rahmat-Samii, *Electromagnetic Band Gap Structures in Antenna Engineering*. Cambridge, U.K.: Cambridge Univ. Press, 2009.

[5] M. Z. Azad and M. Ali, "Novel wideband directional dipole antenna on a mushroom like EBG structure," *IEEE Trans. Antennas Propag.*, vol. 56, no. 5, pp. 1242–1250, May 2008.

[6] D. Qu, L. Shafai, and A. Foroozesh, "Improving microstrip patch antenna performance using EBG substrates," *IEE Proc. Microw. Antennas Propag.*, vol. 153, no. 6, pp. 558–563, 2006.

[7] L. Zhang, J. A. Castaneda, and N. G. Alexopoulos, "Scan blindness free phased array design using PBG materials," *IEEE Trans. Antennas Propag.*, vol. 52, no. 8, pp. 2000–2007, Aug. 2004.

[8] D. F. Sievenpiper, J. H. Schaffner, H. J. Song, R. Y. Loo, and G. Tangonan, "Two-dimensional beam steering using an electrically tunable impedance surface," *IEEE Trans. Antennas Propag.*, vol. 51, no. 10, pp. 2713–2722, Oct. 2003.

[9] D. F. Sievenpiper, "Forward and backward leaky wave radiation with large effective aperture from an electronically tunable textured surface," *IEEE Trans. Antennas Propag.*, vol. 53, no. 1, pp. 236–247, Jan. 2005.

[10] A. Vallecchi, J. R. D. Luis, F. Capolino, and F. D. Flaviis, "Low profile fully planar folded dipole antenna on a high impedance surface," *IEEE Trans. Antennas Propag.*, vol. 60, no. 1, pp. 51–62, Jan. 2012.

[11] L. Akhoondzadeh-Asl, D. J. Kern, P. S. Hall, and D. H. Werner, "Wideband dipoles on electromagnetic bandgap ground planes," *IEEE Trans. Antennas Propag.*, vol. 55, no. 9, pp. 2426–2434, Sep. 2007.

[12] H. Mosallaei and K. Sarabandi, "Antenna miniaturization and bandwidth enhancement using a reactive impedance substrate," *IEEE Trans. Antennas Propag.*, vol. 52, no. 9, pp. 2403–2414, Sep. 2004.

[13] E. Rajo-Iglesias, Ó Quevedo-Teruel, and L. Inclán-Sánchez, "Mutual coupling reduction in patch antenna arrays by using a planar EBG structure and a multilayer dielectric substrate," *IEEE Trans. Antennas Propag.*, vol. 56, no. 6, pp. 1648–1655, Jun. 2008.

[14] T. Nakamura and T. Fukusako, "Broadband design of circularly polarized microstrip patch antenna using artificial ground structure with rectangular unit cells," *IEEE Trans. Antennas Propag.*, vol. 59, no. 6, pp. 2103–2110, Jun. 2011.

[15] D. Sievenpiper, "Artificial impedance surfaces," in *Modern Antenna Handbook*, C. A. Balanis, Ed. New York, NY, USA: Wiley, 2008, ch. 15, pp. 737–777.

[16] K. Sarabandi and N. Behdad, "A frequency selective surface with miniaturized elements," *IEEE Trans. Antennas Propag.*, vol. 55, no. 5, pp. 1239–1245, May 2007.

[17] Q. R. Zheng, Y. Q. Fi, and N. C. Yuan, "A novel compact electromagnetic band-gap (EBG) structure," *IEEE Trans. Antennas Propag.*, vol. 56, no. 6, pp. 1656–1660, Jun. 2008.

[18] J. McVay, N. Engheta, and A. Hoorfar, "Space filling curve high-impedance ground planes," in *Metamaterial Physics and Eng. Explorations*, N. Engheta and R.W. Ziolkowski, Eds. New York, NY, USA: Wiley, 2006, ch. 14, pp. 377–402.

[19] R. Coccioli, F.-R. Yang, K.-P. Ma, and T. Itoh, "Aperture-coupled patch antenna on UC-PBG substrate," *IEEE Trans. Microw. Theory Tech.*, vol. 47, no. 11, pp. 2123–2130, Nov. 1999.

[20] B. Lin, Q. Zheng, and N. Yuan, "A novel planar PBG structure for size reduction," *IEEE Microw. Wireless Compon. Lett.*, vol. 16, no. 5, pp. 269–271, May 2006.

[21] T.-Y. Yun and K. Chang, "Uniplanar one-dimensional photonic-bandgap structures and resonators," *IEEE Trans. Microw. Theory Tech.*, vol. 49, no. 3, pp. 549–551, Mar. 2001.

[22] H. Kim and B. Lee, "Bandgap and slow/fast-wave characteristics of defected ground structures (DGSs) including left-handed features," *IEEE Trans. Microw. Theory Tech.*, vol. 54, no. 7, pp. 3113–3120, Jul. 2006.

[23] C. Caloz, H. Okabe, T. Iwai, and T. Itoh, "A simple and accurate model for microstrip structures with slotted ground plane," *IEEE Microw. Wireless Compon. Lett.*, vol. 14, no. 4, pp. 133–135, Apr. 2004.

[24] A. M. E. Safwat, S. A. Tretyakov, and A. V. Räisänen, "High-impedance wire," *IEEE Antennas Wireless Propag. Lett.*, vol. 6, pp. 631–634, 2007.

[25] S. Xiao, M.-C. Tang, Y.-Y. Bai, S. Gao, and B.-Z. Wang, "Mutual coupling suppression in microstrip array using defected ground structure," *IET Microw. Antennas Propag.*, vol. 5, no. 12, pp. 1488–1494, Dec. 2011.

[26] K. M. K. H. Leong, A. C. Guyette, B. Elamaran, W. A. Shiroma, and T. Itoh, "Coupling suppression in microstrip lines using a bi-periodically perforated ground plane," *IEEE Microw. Wireless Compon. Lett.*, vol. 12, no. 5, pp. 169–171, May 2002.

[27] D.-B. Hou, S. Xiao, B.-Z. Wang, L. Jiang, J. Wiang, and W. Hong, "Elimination of scan blindness with compact defected ground structures in microstrip phased array," *IET Microw. Antennas Propag.*, vol. 3, no. 2, pp. 269–275, 2009.

[28] Y. Horii and M. Tsutsumi, "Harmonic control by photonic bandgap on microstrip patch antenna," *IEEE Microw. Guided Wave Lett.*, vol. 9, no. 1, pp. 13–15, Jan. 1999.

[29] H. Liu, Z. Li, X. Sun, and J. Mao, "Harmonic suppression with photonic bandgap and defected ground structure for a microstrip patch antenna," *IEEE Microw. Wireless Compon. Lett.*, vol. 15, no. 2, pp. 55–56, Feb. 2005.

[30] M. Gustafsson and D. Sjöberg, "Physical bounds and sum rules for high-impedance surfaces," *IEEE Trans. Antennas Propag.*, vol. 59, no. 6, pp. 2196–2204, Jun. 2011.
[31] M. F. Samani and R. Safian, "On bandwidth limitation and operating frequency in artificial magnetic conductors," *IEEE Antennas Wireless Propag. Lett.*, vol. 9, pp. 228–231, 2010.
[32] C. R. Brewitt-Taylor, "Limitation on the bandwidth of artificial perfect magnetic conductor surfaces," *IET Microw. Antennas Propag.*, vol. 1, no. 1, pp. 255–260, 2007.
[33] O. Luukkonen, C. Simovski, G. Granet, G. Goussetis, D. Lioubtchenko, A. Raisanen, and S. Tretyakov, "Simple and accurate analytical model of planar grids and high-impedance surfaces comprising metal strips or patches," *IEEE Trans. Antennas Propag.*, vol. 56, no. 6, pp. 1624–1632, Jun. 2008.
[34] S. Clavijo, R. E. Díaz, and W. E. McKinzie, "High-impedance surfaces: An artificial magnetic conductor for a positive gain electrically small antennas," *IEEE Trans. Antennas Propag.*, vol. 51, no. 10, pp. 2678–2690, Oct. 2003.
[35] A. C. Durgun, C. A. Balanis, and C. R. Birtcher, "Surface wave suppression properties of perforated artificial impedance surfaces," in *Proc. Antennas Propag. Soc. Int. Symp. (APSURSI)*, 2013, pp. 89–90.

Ahmet Cemal Durgun (S'09–M'14) received the B.S.E.E. and M.S.E.E. degrees from Middle East Technical University, Ankara, Turkey, in 2005 and 2008, respectively, where he completed the double major program in mathematics and received the B.S. degree in 2006 and the Ph.D. degree in electrical engineering from Arizona State University, Tempe, AZ, USA, in 2013.

He is currently with the Intel Corporation, Chandler, AZ, USA, working as a Packaging Engineer. His research interests include flexible antennas, high-impedance surfaces, computational electromagnetics, and signal and power integrity for high-speed digital systems.

Constantine A. Balanis (M'68–SM'74–F'86–LF'04) received the B.S.E.E. degree from Virginia Polytechnic Institute and State University, Blacksburg, VA, USA, in 1964, the M.E.E. degree from the University of Virginia, Charlottesville, VA, USA, in 1966, and the Ph.D. degree in electrical engineering from Ohio State University, Columbus, OH, USA, in 1969.

From 1964 to 1970, he was with NASA Langley Research Center, Hampton VA, and from 1970 to 1983 he was with the Department of Electrical Engineering, West Virginia University, Morgantown, WV, USA. Since 1983, he has been with the School of Electrical, Computer, and Energy Engineering, Arizona State University, Tempe, AZ, USA, where he is Regents' Professor. His research interests are in computational electromagnetics, flexible antennas and high-impedance surfaces, smart antennas, and multipath propagation.

Dr. Balanis received an Honorary Doctorate from the Aristotle University of Thessaloniki in 2004, the 2014 LAPC James R. James Lifetime Achievement Award (U.K.), the 2012 Distinguished Achievement Award of the IEEE Antennas and Propagation Society, the 2012 Distinguished Achievement Alumnus Award (College of Engineering, The Ohio State University), the 2005 Chen-To Tai Distinguished Educator Award of the IEEE Antennas and Propagation Society, the 2000 IEEE Millennium Award, the 1996 Graduate Mentor Award of Arizona State University, the 1992 Special Professionalism Award of the IEEE Phoenix Section, the 1989 Individual Achievement Award of the IEEE Region 6, and the 1987–1988 Graduate Teaching Excellence Award, School of Engineering, Arizona State University. He has served as Associate Editor of the IEEE TRANSACTIONS ON ANTENNAS AND PROPAGATION (1974–1977) and the IEEE TRANSACTIONS ON GEOSCIENCE AND REMOTE SENSING (1981–1984); as Editor of the Newsletter for the IEEE Geoscience and Remote Sensing Society (1982–1983); as Second Vice-President (1984) and member of the Administrative Committee (1984–85) of the IEEE Geoscience and Remote Sensing Society; and Distinguished Lecturer (2003–2005), Chair of the Distinguished Lecturer Program (1988–1991), member of the AdCom (1992–95, 1997–1999) and Chair of the Awards and Fellows Committee (2009–2011) all of the IEEE Antennas and Propagation Society. He is the author of *Antenna Theory: Analysis and Design* (Wiley, 2005, 1997, 1982), *Advanced Engineering Electromagnetics* (Wiley, 2012, 1989), and *Introduction to Smart Antennas* (Morgan and Claypool, 2007), and editor of *Modern Antenna Handbook* (Wiley, 2008) and for the Morgan & Claypool Publishers, series on Antennas and Propagation series, and series on Computational Electromagnetics.

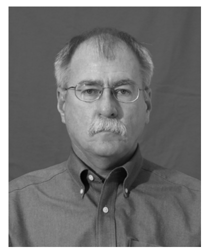

Craig R. Birtcher received the B.S.E.E. and M.S.E.E. degrees from Arizona State University, Tempe, AZ, USA, in 1983 and 1992, respectively.

He has been at Arizona State University since 1987, where he is now an Associate Research Professional in charge of the ElectroMagnetic Anechoic Chamber (EMAC) facility. His research interests include antenna and RCS measurement techniques and near-field to far-field (NF/FF) methods.

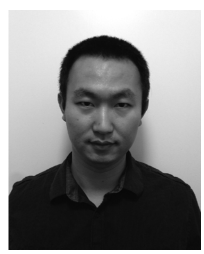

Hai Huang received his B.S. and M.S. in electrical engineering from Tsinghua University, Beijing, China, in 2004 and 2007, respectively, the M.S. degree in electrical engineering from the University of Wisconsin-Madison, Madison, WI, USA, in 2010, and the Ph.D. degree from the School of Electrical, Computer, and Energy Engineering, Arizona State University, Tempe, AZ, USA, in 2014.

His research topics include miniaturized seismometers for Earth and Moon exploration, MEMS accelerometer, flexible, stretchable, foldable electronics and integrated sensors, 3D MEMS-NEMS manufacturing and packaging.

Hongyu Yu (M'94) received the B.S. and M.S. degrees in electronics engineering from Tsinghua University, Beijing, China, in 1997 and 2000, respectively, and the Ph.D. degree in electrical engineering from the University of Southern California, Los Angeles, CA, USA, in 2005.

He joined Arizona State University, Tempe, AZ, USA, in 2008, where he holds a joint position at the School of Earth and Space Exploration and the School of Electrical, Computer, and Energy Engineering as an Associate Professor. His research area is focused on MicroElectroMechanical Systems (MEMS) and other micro systems for earth and space exploration and consumer electronics. His research is to provide portable platforms consumer electronics and instruments for and scientists to explore variety of earth environments and space science, such as micro seismometer and biochemistry liquid sensors for planetary exploration. His current projects also include the manufacturing of high-energy density lithium ion batteries and deformable electronics (including origami electronics) as a universal platforms for consumer products.